# Curvature Dependent Binding of Cytochrome c to Cardiolipin

Margaret M. Elmer-Dixon, †,‡ Ziqing Xie, † Jeremy B. Alverson, † Nigel D. Priestley† and Bruce E. Bowler†,‡,\*

 $^\dagger Department \ of \ Chemistry \ and \ Biochemistry, \ University \ of \ Montana, \ Missoula, \ Montana \ 59812 \ United \ States$ 

**ABSTRACT:** Cytochrome *c* binds cardiolipin on the concave surface of the inner mitochondrial membrane, before oxidizing the lipid and initiating the apoptotic pathway. This interaction has been studied *in vitro*, where mimicking the membrane curvature of the binding environment is difficult. Here we report binding to concave, cardiolipin-containing, membrane surfaces and compare findings to convex binding under the same conditions. For binding to the convex outer surface of cardiolipin-containing vesicles, a two-step structural rearrangement is observed with a small rearrangement detectable by Soret circular dichroism (CD) occurring at an exposed lipid-to-protein ratio (LPR) near 10 and partial unfolding detectable by Trp59 fluorescence occurring at an exposed LPR near 23. On the concave inner surface of cardiolipin-containing vesicles, the structural transitions monitored by Soret CD and Trp59 fluorescence are coincident and occur at an exposed LPR near 58. On the concave inner surface of mitochondrial cristae, we estimate the LPR of cardiolipin to cytochrome *c* is between 50 and 100. Thus, cytochrome *c* may have adapted to its native environment so that it can undergo a conformational change that switches on its peroxidase activity when it binds to CL-containing membranes in the cristae early in apoptosis. Our results show that membrane curvature qualitatively affects peripheral protein-lipid interactions and also highlights the disparity between *in vitro* binding studies and their physiological counterparts where cone-shaped lipids, like cardiolipin, are involved.

## INTRODUCTION

Cytochrome c (Cytc) resides at low millimolar concentrations (0.5 - 1 mM) in the intra-cristal compartments and the intermembrane space of mitochondria.<sup>1,2</sup> The primary functions of Cytc are as a component of the electron transport chain and as a signaling agent in the intrinsic pathway of apoptosis.<sup>3</sup> One of the early signals in the intrinsic pathway of apoptosis involves oxidation of the cone-shaped lipid cardiolipin (CL)<sup>4</sup> by Cytc on the inner mitochondrial membrane (IMM) of the intermembrane space (IMS).<sup>5,6</sup> The IMM, particularly in the intracristal compartments, contains many concave surfaces. 4,7 After oxidation of CL, Cytc is released from the IMM, exits the mitochondria and forms part of the apoptosome in the cytosol, initiating apoptosis.<sup>5,8</sup> Because Cytc-CL binding is a preemptive step to apoptosis, much effort has been directed at elucidating the nature and extent of this interaction. Despite the fact that much of the IMM that Cytc is exposed to has concave curvature, Cytc-CL binding primarily has been studied on the convex outer surface of CL-containing liposomes.<sup>9-12</sup> Here, we investigate Cytc binding to the concave inner surface of pure (100%) CL vesicles to ascertain the effect of membrane curvature on Cytc-CL binding.

In previous work, we showed that yeast iso-1-Cytc binds to the convex surface of 100 nm, pure CL vesicles and reported the associated binding parameters for cooperative, one-site, Langmuir-type binding. <sup>13,14</sup> These studies were carried out at pH 8, conditions selective for binding to the anionic site, A site, <sup>13-15</sup> a site which has long been attributed to electrostatic binding via lysines 72 and 73, <sup>9,16-18</sup> and possibly lysines 86 and 87 (Figure 1a). <sup>19</sup> More recent work suggests that the A site may include other nearby surface lysines (Figure 1a). <sup>14,20</sup> We assigned the two distinct apparent dissociation constants, *K*<sub>d</sub>(app),

found using Soret circular dichroism (CD) and fluorescence spectroscopy, to a two-step conformational rearrangement on the surface of pure CL vesicles (see Table 1, Results). If we interpret the  $K_d$ (app) expressed in units of exposed lipid to protein ratio (LPR) as reflecting the space required on the membrane surface for each conformational rearrangement, the first step requires the surface area of ~10 CL headgroups (~13 nm²; CL headgroup surface area²¹ is 1.298 nm²). This surface area requirement is only slightly larger than the 9.1 nm² of membrane surface area the native state of Cytc is expected to require based on its size,  $^{22,23}$  suggesting only a modest structural rearrangement in the first step.

The second step requires ~23 CL headgroups (~30 nm<sup>2</sup>), indicative of a more significant conformational rearrangement. Fluorescence resonance energy transfer (FRET) studies of partial unfolding on the surface of 1:1 CL:DOPC vesicles, which show that the C-terminal helix moves away from the heme at high LPR,24 are qualitatively consistent with the additional membrane surface area indicated by the  $K_d(app)$  of the second conformational rearrangement we observe on pure CL vesicles. The associated Hill coefficient for each step  $(n \sim 2)$  suggests that iso-1-Cytc interacts directly with two CL headgroups (4 negatively charges) as part of each step of the conformational rearrangement. Studies on horse Cytc binding to the convex outer surface of CL-containing liposomes also have been interpreted in terms of conversion of an initial compact conformer of Cytc to an extended conformer at higher LPR. 11,23-25 Thus, there is a general consensus that Cytc interacts with the convex surface of CL-containing membranes in a two-step process. Cytc undergoes a small conformational rearrangement in the local heme

<sup>&</sup>lt;sup>‡</sup>Center for Biomolecular Structure and Dynamics, University of Montana, Missoula, Montana, 59812, United States

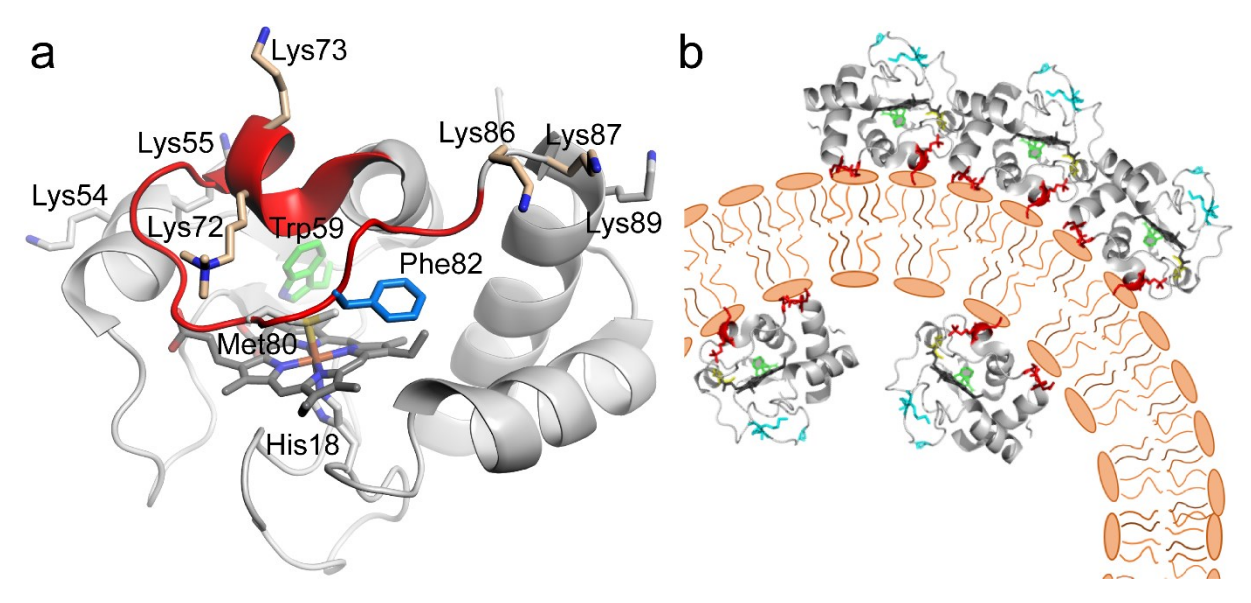


Figure 1. (a) Yeast iso-1-Cytc (PDB ID: 2YCC) showing lysines 72, 73, 86 and 87 (tan stick models), which are commonly assigned as constituents of the A-site. Nearby lysines 54, 55 and 89 are also shown. Trp59 is shown in green behind the heme. Phe82 is shown in blue in front of the heme. The heme and its ligands, Met80 and His18, are also shown. (b) Schematic representation of spatial constraints on binding iso-1-Cytc to the convex outer surface versus the concave inner surface of a pure CL vesicle. The relative sizes of the vesicle (100 nm diameter) and Cytc (3 nm diameter) used in the experiment are not drawn to scale so that protein structural details could be retained. Thus, the curvature of the vesicle relative to the protein in this image is exaggerated.

environment, readily detectable by Soret CD, <sup>11,13,14,25</sup> when it is bound to a crowded membrane surface. As the membrane surface becomes less crowded, Cyt*c* partially unfolds. This larger conformational change is detected by a significant increase in Trp59 fluorescence as the Trp59 distance from the heme increases. <sup>11,13,14,25</sup>

Conformational rearrangements of proteins on a concave membrane surface differ in two respects relative to those on a convex surface. A convex surface curves away from a protein bound to it, which should diminish steric clashes between adjacent proteins on the surface relative to a concave surface which curves toward bound proteins (Figure 1b). For the 100 nm CL vesicles used here, steric crowding on the inner leaflet increases by 16% as assessed by the membrane surface area occluded by each Cytc molecule at saturation binding (Supporting Information, Table S1). Thus, more surface area is necessary for protein binding to a concave membrane surface. The concave membrane surface will also better match the curvature of a globular protein. So, one might expect that more of the protein could interact with the membrane perhaps increasing the number of lipids which directly bind to the protein and thus the cooperativity of binding and/or structural rearrangements on the membrane surface.

# RESULTS

Entrapping iso-1-Cytc within the Vesicle Lumen. To examine protein binding to concave membrane surfaces, we developed methods to encapsulate wild-type (WT, carries a C102S mutation to prevent intermolecular disulfide dimerization) iso-1-Cytc molecules within 100 nm, pure CL vesicles, so that they only see the concave surface of the bilayer. Vesicles were formed in the presence of WT iso-1-Cytc in high salt to guarantee minimal electrostatic binding of the protein to the outer membrane surface. After extrusion, external iso-1-Cytc was removed by cation-exchange chromatography. Because

vesicles need to be formed in the presence of NaCl, the ionophore nonactin<sup>26</sup> was included during formation of liposomes so that NaCl could later be removed from the vesicle lumen. Vesicle titrations of Cytc binding to the convex exterior surface of CL-containing vesicles are typically done at constant protein concentrations between 5 and  $10~\mu M^{11,13,14,17,18,25,27}$  in the presence of increasing amounts of vesicles. For titrations as a function of exposed LPR for iso-1-Cytc trapped inside vesicles, iso-1-Cytc concentration must be changed to vary exposed LPR because the number of exposed lipids on the inner leaflet of a 100 nm vesicle is constant. To achieve exposed LPR across the same range as for titrations of the convex outer surface of vesicles with iso-1-Cytc, the vesicles must be formed in the presence of iso-1-Cytc at concentrations ranging from approximately 0.5 – 5 mM (Table S2). Thus, the concentration of iso-1-Cytc in the lumen of the pure CL vesicles in this study is similar to that observed physiologically in the IMS of mitochondria.<sup>1,2</sup>

Effect of LPR on iso-1-Cytc Conformation on a Concave Membrane Surface. To monitor local and global structural rearrangement as a function of exposed LPR, Soret CD and Trp59 fluorescence spectroscopy, respectively, were used. Soret CD is sensitive to the local heme environment, including distortion of the heme from planarity caused, in part, by its CXXC attachment sequence<sup>28</sup> and coupling interactions with nearby aromatic residues<sup>29</sup> such as Phe82 (see Fig. 1a).<sup>30</sup> Trp59 fluorescence depends on the Trp59-heme distance (see Fig. 1a) and is used to monitor changes in the tertiary structure of Cytc.<sup>31</sup> For binding titrations followed by Soret CD, the CL vesicle titration evaluated iso-1-Cytc binding from low exposed LPR (high iso-1-Cytc concentration, Fig. 2a, blue spectrum) to high exposed LPR (low protein concentration, Fig. 2a red spectrum) to assess the effect of the binding density of iso-1-Cytc on the concave inner surface of the CL vesicles on the local heme environment. Notably, the largest perturbation to the Soret CD spectrum occurs at the lowest concentration of iso-1-Cytc in the vesicle lumen. By contrast, at the highest concentration of iso-1-

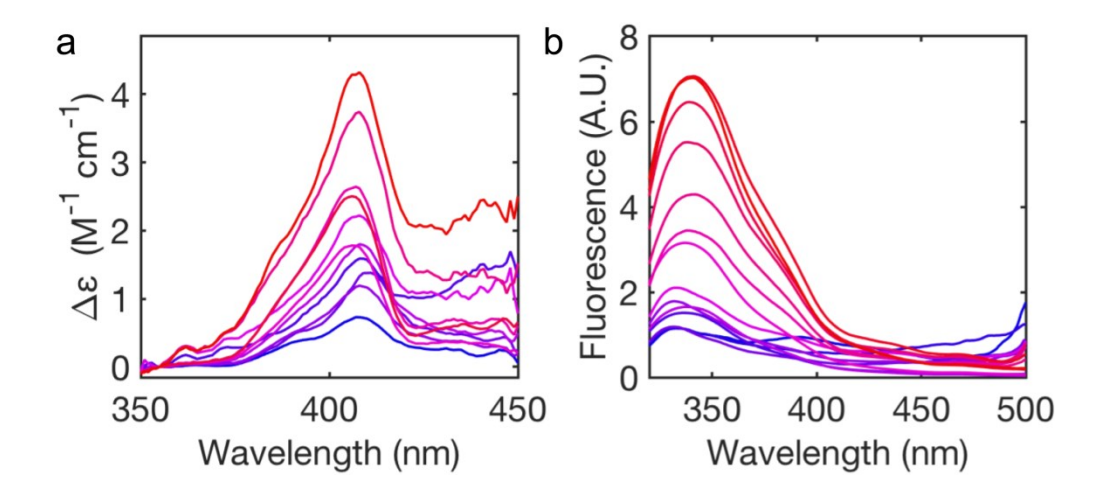
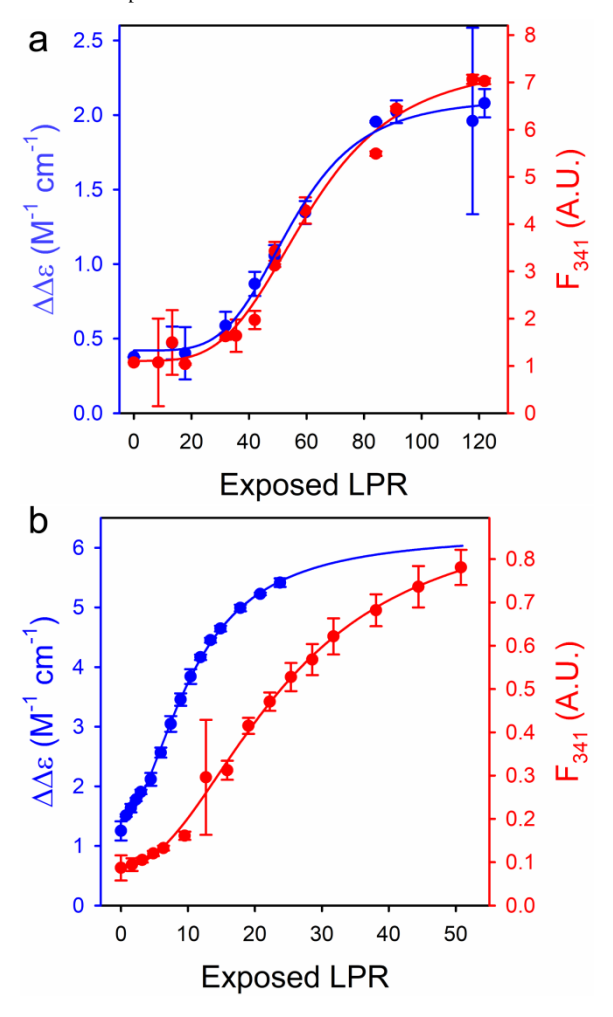


Figure 2. (a) Soret CD spectra and (b) Trp59 fluorescence spectra of iso-1-Cytc from low exposed LPR (high iso-1-Cytc concentration in vesicle lumen; blue spectrum is iso-1-Cytc in the absence of vesicles) to high exposed LPR (red, low iso-1-Cytc concentration in vesicle lumen) inside 100 nm, 100% CL vesicles. Vesicle concentration was adjusted, so that iso-1-Cytc concentration was 10  $\mu$ M for CD spectra and 5  $\mu$ M for fluorescence spectra. Buffer for all measurements was 20 mM TES buffer, 0.1 mM EDTA at pH 8.



**Figure 3.** Binding curves for WT iso-1-Cytc interacting with the (a) inner concave surface and (b) the outer convex surface of 100% CL vesicles. Average Soret CD amplitude ( $\Delta\Delta\epsilon$  =  $\Delta\epsilon_{406}$  –  $\Delta\epsilon_{420}$ , solid blue circles) and average Trp59 fluorescence at the emission maximum of 341 nm (F<sub>341</sub>, solid red circles) as a function of exposed LPR. Solid curves are fits to Eq. 1 in Methods. The error bars of the data points are the standard deviation from three independent trials. Data in part (b) are taken from ref. 14.

Cytc within the vesicle lumen, the perturbation of the Soret CD spectrum is modest. The lowest concentration of iso-1-Cytc within the lumen of the vesicles is >10-fold higher than the  $K_d$ reported for Cytc binding at pH 8.15 So, binding to the surface is expected to be complete at all Cytc concentrations. At 5 mM protein concentration, ~1300 iso-1-Cytc molecules would be contained inside a 100 nm CL vesicle. If we assume 9.1 nm<sup>2</sup> is required per iso-1-Cytc molecule<sup>22,23</sup> about 40% of the surface area of the inner leaflet of the vesicle would be needed to bind all iso-1-cytc molecules. Given site exclusion and entropy effects,<sup>32</sup> it is possible that a small fraction of the iso-1-Cytc may be unable to bind to the CL membrane surface at this highest concentration, but most iso-1-Cytc will be bound. Thus, the Soret CD data demonstrate that when the membrane surface is crowded with protein, the structural perturbation to iso-1-Cytc is small and when considerable space is available (for 0.5 mM iso-1-Cytc in the vesicle lumen, surface coverage of the inner leaflet is about 4%) on the surface of the membrane, a structural rearrangement of iso-1-Cytc occurs.

Trp59 fluorescence as a function of exposed LPR on the concave inner surface of pure CL vesicles is shown in Figure 2b. At the highest iso-1-Cytc concentration when the surface of the inner leaflet is crowded, Trp59 emission is quenched by the heme indicating that the protein has a compact folded structure with Trp59 near the heme (see Fig. 1a). As the concentration of iso-1-Cytc within the vesicle decreases, Trp59 emission increases. Thus, as more space becomes available on the surface of the membrane, iso-1-Cytc unfolds. The data also show that unfolding of Cytc on the surface of a CL-containing membranes could occur at physiologically-relevant concentrations of Cytc.<sup>1,2</sup>

Surface Area Requirements and Cooperativity of iso-1-Cytc Conformational Transitions on a Concave Membrane Surface. The amplitude of the CD signal ( $\Delta\Delta\epsilon = \Delta\epsilon_{406} - \Delta\epsilon_{420}$ ) was plotted versus exposed LPR and fit to a one-site cooperative Langmuir binding model (Eq. 1 in Methods) to determine  $K_{\rm d}$ (app) and n (Fig. 3a, Table 1). Compared to binding titrations on the external convex surface of pure 100 nm CL vesicles,  $K_{\rm d}$ (app) obtained from Soret CD measurements on the concave inner surface of pure CL vesicles is much higher (Table 1), indicating that more space is required for the Soret CD-monitored conformational change on a concave versus a convex surface.

Table 1. Thermodynamic parameters for iso-1-Cytc binding to 100% CL vesicles.<sup>a</sup>

|                       | CD   |              | Fluorescence   |              |
|-----------------------|--|--------------|--|--------------|
| Membrane<br>Curvature | K <sub>d</sub> (app),<br>Exposed<br>LPR <sup>b</sup> | n            | K <sub>d</sub> (app),<br>Exposed<br>LPR <sup>b</sup> | n            |
| Concave               | 55 ± 2   | 4.4 ±<br>0.6 | 61 ± 3   | 3.7 ±<br>0.6 |
| Convex <sup>c</sup>   | 10.2 ± 0.2   | 2.2 ±<br>0.1 | 23.4 ± 0.8   | 2.3 ± 0.2    |

<sup>a</sup>Reported errors are the standard error in the fit of the parameter. <sup>b</sup>For concave curvature the exposed leaflet is the inner leaflet. For convex membrane curvature, the exposed leaflet is the outer leaflet. <sup>c</sup>Parameters are from ref. 13.

The associated Hill coefficient, n, is also twice the value reported for binding on a convex membrane surface. The increase in Trp59 fluorescence intensity at the emission maximum (341 nm) was plotted versus exposed LPR and fit to Eq. 1 to obtain  $K_d(app)$  and n (Fig. 3a, Table 1). The  $K_d(app)$  and n values obtained for binding on the concave inner surface of pure CL vesicles from Trp59 fluorescence data are approximately double the magnitude of the values obtained for Cytc-CL binding on the convex exterior surface of pure 100 nm CL vesicles (Table 1). Whereas the  $K_d(app)$  and n parameters obtained from Soret CD versus Trp59 fluorescence data are significantly different for binding to convex membrane surfaces, they are essentially identical for binding to concave surfaces (Table 1). Thus, conformational rearrangement of iso-1-Cytc is concerted on the concave inner surface (Fig. 3a) and stepwise on the convex outer surface (Fig. 3b) of 100 nm pure CL vesicles.

The lowest exposed LPR in the titration followed by Soret CD in Figure 3a gives a spectrum similar to the spectrum of iso-1-Cytc free in solution at pH 8 (see Fig. 4). Both Soret CD spectra are consistent with significant population of the alkaline conformer of iso-1-Cytc where the Met80 heme ligand is replaced by lysine 72, 73 or 79.<sup>33</sup> This result is not surprising because the midpoint pH for the alkaline transition of WT iso-1-Cytc expressed from *Escherichia coli* is 8.<sup>33</sup> By contrast at an exposed LPR near 23, the negative band of the Soret CD of iso-1-

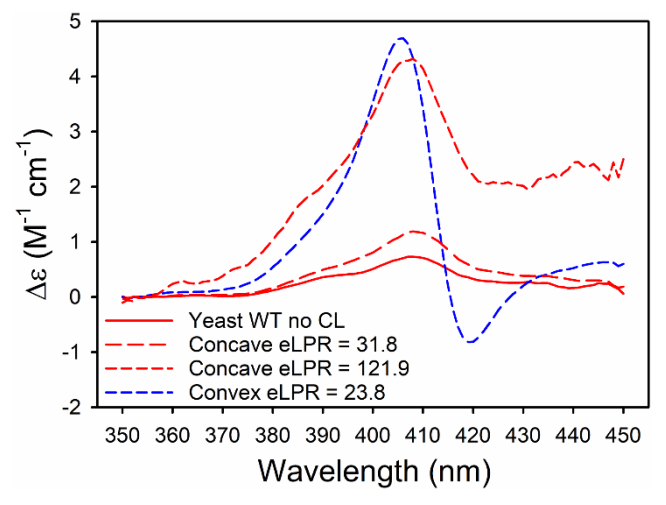


**Figure 4.** Comparison of Soret CD spectra of WT yeast iso-1-Cyte bound to the concave (inner leaflet) versus the convex (outer leaflet) of 100 nm CL vesicles. Exposed lipid to protein ratio (eLPR) of each

spectrum is given in the figure legend. The convex spectrum was previously reported in Fig. S3 of ref. 14.

Cytc near 420 nm, typical of the native conformer free in solution, reappears when WT iso-1-Cytc is bound to the convex exterior surface of pure CL vesicles (Figure 4). Thus, the initial structural rearrangement that occurs on the outer surface of pure CL vesicles, which appears to make the structure of iso-1-Cytc more nativelike, does not occur on the concave inner surface of pure CL vesicles. Instead, the protein appears to maintain a heme environment that is more similar to that of the protein free in solution up to an exposed LPR of almost 40 (Fig. 4). At low exposed LPR maintaining the lysine ligation of the alkaline state will decrease peroxidase activity, <sup>34</sup> perhaps providing a better off state for peroxidase activity at low exposed LPR.

#### DISCUSSION

Effect of Crowding on the Conformation of Cytc on Mem**brane Surfaces.** Most studies of binding of Cytc to CL vesicles hold the concentration of Cytc constant and vary the concentration of vesicles making it more difficult to distinguish structural changes due to the initial binding event from those due to crowding on the surface of the vesicle. Recent single molecule studies indicate that the  $K_d$  for Cytc binding to CL membrane surfaces is near the 10 µM Cytc concentration often used for titrations with CL-containing vesicles because of the sensitivity of the Soret CD and Trp59 fluorescence spectroscopic probes. By encapsulating Cytc within CL vesicles, we can vary the concentration of Cytc within the vesicle lumen simply by varying the initial concentration of Cytc present when the vesicles are produced. The overall concentration of Cytc in the solution can then be adjusted to the appropriate range for spectroscopic measurements by simply diluting the vesicles by the appropriate amount. For the experiments presented here, the iso-1-Cytc concentrations used at each exposed LPR (Table S2) are well above the K<sub>d</sub> of Cvtc for binding to CL membranes. Thus, Cvtc is fully bound to the CL surface throughout the titrations in Figures 2 and 3a. The observed conformational change reflects crowding on the membrane surface. In other words, the conformational change corresponds to step 2 (partial unfolding monitored by Trp59 fluorescence) for titrations of Cytc with the convex surface of CL vesicles (see Fig. 3b). In our experiments, we observe that partial unfolding occurs as the concentration of iso-1-Cytc in the vesicle lumen decreases and more space becomes available on the membrane surface. This result is important because it provides a clear and direct validation of binding models which link the equilibrium for partial unfolding of Cytc on the membrane surface to the degree of crowding on CL membrane surfaces.25

Direct tests of the effect of crowding on the conformational distribution of compact versus partially unfolded conformers of Cytc bound to the outer convex surface of 50 nm diameter CLcontaining vesicles have been done using apo-Cytc to crowd the membrane surface.<sup>23</sup> The distribution of compact versus extended structure, as detected by intramolecular FRET using dansyl-labeled holo-Cytc, was only modestly affected, even at apo-Cytc concentrations that limited the space per Cytc molecule on the membrane to that needed for a fully folded Cytc. Given our results for binding to a concave surface, this result suggests that crowding is less effective on convex membrane surfaces than on concave surfaces. However, the possibility that apo-Cytc, which is disordered, has a qualitatively different effect on the conformational distribution of dansyl-labeled holo-Cytc bound to a membrane surface than when an ordered globular protein is used to crowd the surface cannot be ruled out.

Iso-1-Cytc Requires More Space for Conformational Rearrangements on Concave Membrane Surfaces. The concerted partial unfolding on the concave inner surface occurs at about twice the exposed LPR ( $K_d(app)$  of ~58, Table 1) of the second conformational rearrangement (partial unfolding) on the convex outer surface of pure CL vesicles. This  $K_d(app)$  corresponds to a surface area of  $\sim$ 73 nm<sup>2</sup> for partial unfolding on the concave inner surface of pure CL vesicles, more than twice the surface area needed for this conformational rearrangement on the convex outer surface of pure CL vesicles. The Hill coefficient, n, is approximately the sum of the individual steps observed for binding to a convex membrane surface. However, for convex titrations, it is the lipid concentration that is being varied, whereas for concave titrations iso-1-Cytc concentration is being varied. Thus, the cooperativity relates to an attribute of iso-1-Cytc, perhaps the number of lysines (~4) that bind to the CL membrane surface when iso-1-Cytc unfolds.

One factor that may lead to the concerted (concave surfaces) versus the stepwise (convex surfaces) mechanism for structural rearrangement of iso-1-Cytc on the membrane surface is that the concave surface is more stable because the cone-shape of CL is better adapted to a concave surface. Our recent studies showing that CL preferentially partitions to the inner leaflet of 100 nm vesicles supports this contention.<sup>35</sup> A more stable surface would be less prone to deformation and thus require more points of contact to initiate structural rearrangement of iso-1-Cytc. The concave curvature may in turn facilitate simultaneous contact with lysine residues in or near the A site because the curvature of the surface allows for closer contact with more of the surface of iso-1-Cytc. This tension between a surface that is harder to deform and the ability of iso-1-Cytc to form more contacts with the surface because of the complementary curvatures may explain the cooperative one-step structural transition with the Soret CD and Trp59 fluorescence monitored transitions occurring simultaneously (Figure 3a, Table 1). The convex exterior surface of a vesicle, by contrast, curves away from the surface of Cytc allowing fewer of its lysines to interact with CL molecules simultaneously. Even when the surface is crowded, the protein might have to undergo a small structural rearrangement to interact effectively with the convex surface. The CL molecules on a convex surface are also more poorly packed because of their cone shape. These factors may favor a two-step structural rearrangement because the looser packing of CL more readily allows the initial small local structural rearrangement detectable by Soret CD (Figure 3b, Table 1).

The larger surface area  $(K_d(app))$  needed for partial unfolding of iso-1-Cytc on a concave versus a convex membrane surface likely has several contributing factors. One factor, as illustrated in Figure 1b, is that a concave surface curves towards bound proteins which will enhance steric interaction between adjacent proteins leading to more excluded volume on a concave surface and thus a requirement for more lipid surface area to allow structural rearrangements. If we assume the effective radius of Cytc doubles in the partially unfolded form of Cytc, our model in the Supporting Information for steric effects on concave versus convex surfaces indicates that sterics will be 35% more demanding on the concave versus the convex surface (Table S1). The combination of the cone-shape of CL being better adapted to the concave curvature and thus less prone to deformation and greater excluded volume effects between Cytc molecules likely combine to cause the  $\sim 2.5$ -fold higher  $K_d$ (app) (larger membrane surface area) needed to partially unfold iso-Cytc on the concave versus the convex membrane surface as detected by Trp59 fluorescence (Table 1).

Our recent work on the effect of Lys→Ala variants of iso-1-Cytc on binding to the convex outer surface of pure CL vesicles shows that at least four lysines govern binding at the A site (Lys72, Lys73, Lys86, and Lys87). 14 The results also indicate that neighboring lysines (Lys54, Lys55 and Lys89, see Fig 1a) also could be involved in A site binding. 14 Thus, a large surface of lysines likely contributes to electrostatic binding via the A site.<sup>20</sup> The better shape complementarity between the concave inner surface of a CL vesicle and the surface of iso-1-Cytc may facilitate contact with a larger group of these lysines and the negatively-charged CL headgroups leading to a larger structural rearrangement on a concave versus a convex membrane surface. Further investigation of which lysines contribute to A-site binding will be important, as will determination of whether the relative importance of each lysine contributing to the A site is the same on convex versus concave surfaces.

A recent study showed that slow gradual (SG) addition of CL to iso-1-Cytc over an LPR range of 0 to 10 versus large more abrupt (LA) additions of CL to iso-1-Cytc over an LPR of 0 to 60 appeared to affect the mechanism of interaction of iso-1-Cytc with CL.<sup>36</sup> In particular, the LA scheme shifted the structural transitions observed spectroscopically to higher LPR. Because we prepare samples of iso-1-Cytc encapsulated in CL vesicles individually, the addition of CL could be viewed as LAlike and possibly explain the higher exposed LPR we observe for interaction of iso-1-Cytc with the concave inner surface of CL vesicles. However, the number of CL molecules on the inner leaflet of a 100 nm CL vesicle is fixed. We are titrating the number of molecules of iso-1-Cytc in the lumen of the vesicle in our experiment while CL remains fixed. In our previous work on binding of iso-1-Cytc to the outer convex surface of CL vesicles, each sample of the titration was prepared separately and thus the additions of 100 nm CL vesicles to each iso-1-Cytc solution also could be viewed as large and abrupt. So, the differences in the  $K_d(app)$  in Table 1 for convex versus concave CL membrane surfaces are best attributed to a change in the mechanism of binding due to the concave versus the convex curvature of the membrane surfaces.

Relevance for Cytc:CL Binding in Mitochondria. Many studies of Cytc binding to CL-containing liposomes indicate that Cytc unfolds at high LPR<sup>11,13,14,23-25</sup> leading to an increase in the peroxidase activity of Cytc that acts as a signaling agent in the early stages of apoptosis. 6 Other studies have questioned the physiological relevance of Cytc unfolding on CL-containing membranes. 10,37 Although much of the surface of the IMM is concave, 4,7 most of these studies measured binding to the convex outer surface of CL liposomes. In their work on binding of horse Cytc to the concave surface of reverse micelles titrated with CL, Wand and colleagues found no evidence of partial unfolding of Cytc. This conclusion was based on the observation that there are only small changes in the <sup>1</sup>H-<sup>15</sup>N HSQC of horse Cytc during the CL titration. 10 The diameter of the reverse micelles in this study was about 4 nm. If the entire surface area of the reverse micelle was replaced by CL during the titration, maximally 35 – 40 CL could be accommodated on the available surface area. At the 7 mM concentration of horse Cytc used in these experiments, each reversed micelle would contain no more than one Cytc molecule. Thus, the maximal value for the exposed LPR would be 35 – 40 and is probably less. Our data (Fig. 3a) also show minimal structural perturbation to iso-1-Cytc at exposed LPR values less than 40.

For mitochondria in the orthodox state, the diameters of the cristae and the cristae junctions are near 30 nm. <sup>7,38,39</sup> At this diameter, steric effects on Cyte bound to the inner convex surface

are expected to exceed those on the outer concave surface by 76% (Table S1). The intra-cristal regions make up most of the surface area of the IMM available to Cytc, providing substantial surface area with negative curvature.<sup>38</sup> The negative curvature of the cristae fall in between that of the 4 nm reversed micelles used by Wand and colleagues and the 100 nm CL vesicles used here. Both experiments indicate that, at exposed LPR below 40, partial unfolding does not occur on concave CL-containing membrane surfaces. However, our data show that at physiological concentrations of Cytc (0.5 – 1.0 mM, high exposed LPR in our study), partial unfolding could occur on the concave surfaces of the intra-cristal compartments of the IMM. For a cylindrical cristae with a length of 300 nm, assuming 25% of the surface area is occupied by CL, Cytc concentrations of 0.5 - 1.0mM would yield CL to Cytc ratios (LPR) of 50 - 100. Thus, the data presented here indicate that partial unfolding of Cytc could occur under physiologically relevant conditions.

It is important to note that the pH of the IMS is  $6.88 \pm 0.08$ . Our experiments were carried out at pH 8 so that Cytc binding to the CL membrane surface would involve primarily the electrostatic A site. <sup>13-15</sup> At the pH of the IMS, binding of Cytc to CL membranes will also involve site L, <sup>12</sup> and a hydrophobic component, often referred to as site C. <sup>16</sup> At pH 8, the population of the alkaline state of WT yeast iso-1-Cytc also is about 50%. <sup>33,41</sup> Therefore, the structural changes we observe when Cytc binds to the concave inner surface of a pure CL vesicle at pH 8 may differ from those that occur on the concave surface of mitochondrial cristae. However, our results show that membrane curvature and the density of Cytc on the membrane surface will be important components of the interaction of Cytc with CL membranes *in vivo*. Future experiments will interrogate the effect of pH on the binding of Cytc to concave CL surfaces.

# CONCLUSIONS

Our findings indicate that Cytc partially unfolds on both convex and concave surfaces of pure CL vesicles. However, the membrane surface area required for partial unfolding is larger on concave than on convex membrane surfaces. The unfolding process is also concerted on a concave surface versus the twostep structural rearrangement observed on a convex membrane surface. The larger surface area required on the concave versus the convex surface suggests that the extent of protein unfolding on concave surfaces may be more extensive than for convex surface binding. Our calculation of the effect of vesicle radius on differential steric effects on concave versus convex surfaces show that the small diameter and concave curvature of the mitochondrial cristae could have an important impact on the LPR needed for conformational rearrangements of Cytc on CLcontaining membranes and thus in controlling the peroxidase activity of Cytc in the early stages of apoptosis.

# **METHODS**

**Sample Preparation.** WT (C102S mutation to prevent intermolecular disulfide dimerization) yeast iso-1-Cytc was expressed from *Escherichia coli* BL21 DE3 cells (BioRad, Phage T1-resistant strain) and purified following previously reported methods. <sup>13</sup> Protein was concentrated to between about 0.5 and 5 mM in 20 mM TES, 0.1 mM EDTA, 0.1 M NaCl, pH 8. For each titration point, three aliquots of 100% CL (Avanti Polar Lipids, Inc) (minimally 5 mg each) were mixed with the ionophore Nonactin<sup>26</sup> in a 100:1 ratio, and the mixtures were dried individually under compressed nitrogen for approximately 2 hours to remove chloroform. The lipid/nonactin mixture was

then combined with a volume of concentrated protein solutions to form vesicles that yielded a lipid concentration of 5 mM (Table S2). Mixing was performed at low speeds on a vortexer. Vortexing was sufficiently vigorous to thoroughly mix the protein with the CL/nonactin but not so vigorous that formation of bubbles occurred. Protein/lipid/nonactin mixtures were extruded to 100 nm using an Avanti Mini Extruder where two 100 nm membrane supports were used for extrusion and samples were passed through the extruder 11 times. After extrusion, samples were loaded onto a washed (20 mM TES buffer, 0.1 mM EDTA, pH 8) CM Sepharose Fast Flow column (GE Healthcare Life Sciences) and run down the column in the mobile phase. Cytc external to the vesicles bound to the CMsepharose cation-exchange resin while the negatively-charged vesicles filled with Cytc eluted off the column. Eluent containing Cytc filled vesicles was collected and concentrated to <1 mL using Amicon Ultra-15 Centrifugal Filter Units with 50k MWCO (EMD Millipore, Sigma). Samples were diluted to 15 mL in 20 mM TES Buffer, 0.1 mM EDTA, pH 8 and set to equilibrate on an orbital shaker for 8 hours at 4 °C. Conductivity was periodically measured to follow the flow of NaCl from inside the vesicles via the ionophore nonactin. When conductivity stabilized, indicating that the flow of NaCl out of the interior of the samples was complete, the CL vesicles loaded with iso-1-Cytc were again run down a CM Sepharose column in 20 mM TES Buffer, 0.1 mM EDTA, pH 8, collected and concentrated using the same 50k MWCO ultrafiltration devices. Conductivity at equilibrium was approximately the conductivity of 20 mM TES, 0.1 mM EDTA buffer at pH 8. The concentration of iso-1-Cytc was measured with a Beckman Coulter DU800 using previously reported extinction coefficients, 42 and taking into account scattering off of the vesicles. A Malvern Zetasizer was used to perform Dynamic Light Scattering on all samples to determine vesicle size. Vesicle size was measured to be 100 nm  $\pm$ 5 nm for all replicates at all titration points. Vesicle size was used to calculate lipid concentration and determine exposed LPR for each protein concentration point using a method based on Mie scattering (Table S2). 43,44 The Mie scattering method has been validated by phosphorous analysis.44 The fits to the scattering profiles were consistent with a narrow particle size distribution centered around 100 nm. Samples were then diluted to either 5 µM or 10 µM iso-1-Cytc concentration, as appropriate, for spectroscopic measurements.

Circular Dichroism Spectroscopy. Soret CD spectra were measured using previously reported methods. <sup>13</sup> Briefly, CD data were acquired using an Applied Photophysics Chirascan Spectrophotometer to measure the spectral region from 350 nm – 450 nm, scanning in 1 nm steps with a 3 second/nm scan rate and 1.8 nm bandwidth. Samples were contained in a 4 mm by 10 mm Hellma cuvette (Hellma Analytics) utilizing the 4 mm pathlength. Spectra were smoothed with a 6-point Savitsky-Golay smoothing function and data were analyzed using the difference between the positive maximum near 406 nm and negative minimum near 420 nm as the signal amplitude, as previously described. <sup>13,14</sup>

**Tryptophan Fluorescence Spectroscopy.** Trp59 fluorescence measurements were performed using previously reported methods. <sup>13</sup> Briefly, fluorescence data were acquired using an Applied Photophysics Chirascan Spectrophotometer modified for fluorescence data acquisition using a scanning emission monochromator (Applied Photophysics). Samples were excited at 295 nm (5 nm bandwidth) and fluorescence was measured at 90° with a 305 nm cutoff filter (Newport Corp) in-line to limit excitation bleed through. Emission was measured from 320 nm

to 500 nm in 1 nm steps, with 0.5 sec per step and a 2.5 nm bandwidth. A 5 mm by 5 mm Hellma fluorescence cuvette was used for measurements. Spectra were smoothed with a 6-point Savitsky-Golay smoothing function and data were analyzed to extract fluorescence peak emission intensity as previously reported. <sup>13,14</sup>

**Data Fitting.** A one site cooperative Langmuir-type equation (Eq. 1) was used to fit CD and fluorescence data, where the spectroscopic value, s(x)

$$s(x) = \frac{s_o + s_1 \left(\frac{x}{K_d(\text{app})}\right)^n}{1 + \left(\frac{x}{K_d(\text{app})}\right)^n} \quad (1)$$

corresponds to the amplitude measured at the exposed LPR, x, in the titration and  $s_0$  and  $s_1$  are the amplitudes of the initial (free protein) and final (lipid bound protein) states, respectively. Here,  $K_d$ (app) is the apparent dissociation constant corresponding to the exposed LPR required to induce half occupancy of the conformation associated with site A binding to CL and n is the associated Hill coefficient.

## ASSOCIATED CONTENT

#### **Supporting Information**

The Supporting Information is available free at <a href="http://pubs.acs.org">http://pubs.acs.org</a>. A method for calculating the increased steric crowding on the concave inner leaflet versus the convex outer leaflet of CL vesicles is described. Table S1 summarizes the results of these calculations. Table S2 provides details of preparation of iso-1-Cytc encapsulated within 100 nm CL vesicles including CL concentration measured by Mie scattering and determination of exposed LPR.

## **AUTHOR INFORMATION**

# **Corresponding Author**

\*Bruce E. Bowler - Department of Chemistry and Biochemistry and Center for Biomolecular Structure and Dynamics, University of Montana, Missoula, Montana 59812, United States; orcid.org/0000-0003-1543-2466; Phone: (406) 243-6114; Email: bruce.bowler@umontana.edu; Fax: (406) 243-4227.

# Authors

Margaret Elmer-Dixon - Department of Chemistry and Biochemistry and Center for Biomolecular Structure and Dynamics, University of Montana, Missoula, Montana 59812, United States. Present Address: Department of Physics, University of Minnesota – Duluth, Duluth, MN 55812; orcid.org/0000-0001-5261-2576.

Ziqing Xie - Department of Chemistry and Biochemistry, University of Montana, Missoula, Montana 59812, United States.

Jeremy B. Alverson - Department of Chemistry and Biochemistry, University of Montana, Missoula, Montana 59812, United States; orcid.org/0000-0003-0898-2582.

Nigel D. Priestley - Department of Chemistry and Biochemistry, University of Montana, Missoula, Montana 59812, United States; orcid.org/0000-0002-2791-0958.

## Notes

The authors declare no competing interest.

## ACKNOWLEDGMENT

This work was supported by grants from the NSF [CHE-1609720 and CHE-1904895 (B.E.B)].

#### REFERENCES

- (1) Hackenbrock, C. R.; Chazotte, B.; Gupte, S. S., The random collision model and a critical assessment of diffusion and collision in mitochondrial electron transport, *J. Bioenerg. Biomembr.* **1986**, *18*, 331-368. https://doi.org/10.1007/BF00743010.
- (2) Morales, J. G.; Holmes-Hampton, G. P.; Miao, R.; Guo, Y.; Münck, E.; Lindahl, P. A., Biophysical characterization of iron in mitochondria isolated from respiring and fermenting yeast, *Biochemistry* **2010**, *49*, 5436–5444. https://doi.org/10.1021/bi100558z.
- (3) Alvarez-Paggi, D.; Hannibal, L.; Castro, M. A.; Oviedo-Rouco, S.; Demicheli, V.; Tórtora, V.; Tomasina, F.; Radi, R.; Murgida, D. H., Multifunctional cytochrome *c*: learning new tricks from an old dog, *Chem. Rev.* **2017**, *117*, 13382–13460.
- (4) Ikon, N.; Ryan, R. O., Cardiolipin and mitochondrial cristae organization, *Biochim. Biophys. Acta Biomembr.* **2017**, *1859*, 1156-1163.
- (5) Orrenius, S.; Zhivotovsky, B., Cardiolipin oxidation sets cytochrome *c* free, *Nat. Chem. Biol.* **2005**, *1*, 188-189. https://doi.org/10.1038/nchembio0905-188.
- (6) Kagan, V. E.; Tyurin, V. A.; Jiang, J.; Tyurina, Y. Y.; Ritov, V. B.; Amoscato, A. A.; Osipov, A. N.; Belikova, N. A.; Kapralov, A. A.; Kini, V.; Vlasova, I. I.; Zhao, Q.; Zou, M.; Di, P.; Svistunenko, D. A.; Kurnikov, I. V.; Borisenko, G. G., Cytochrome *c* acts as a cardiolipin oxygenase required for release of proapoptotic factors, *Nat. Chem. Biol.* **2005**, *1*, 223-232. https://doi.org/10.1038/nchembio727.
- (7) Frey, T. G.; Renken, C. W.; Perkins, G. A., Insight into mitochondrial structure and function from electron tomography, *Biochim. Biophys. Acta* **2002**, *1555*, 196-203.
- (8) Jiang, X.; Wang, X., Cytochrome *c*-mediated apoptosis, *Annu. Rev. Biochem.* **2004,** 73, 87-106. https://doi.org/10.1146/annurev.biochem.73.011303.073706.
- (9) Rytömaa, M.; Kinnunen, P. K. J., Reversibility of the binding of cytochrome *c* to liposomes, *J. Biol. Chem.* **1995**, *270*, 3197-3202.
- (10) O'Brien, E. S.; Nucci, N. V.; Fuglestad, B.; Tommos, C.; Wand, A. J., Defining the apoptotic trigger: the interaction of cytochrome c and cardiolipin, *J. Biol. Chem.* **2015**, *290*, 30879-30887.
- (11) Pandiscia, L. A.; Schweitzer-Stenner, R., Coexistence of native-like and non-native partially unfolded ferricytochrome *c* on the surface of cardiolipin-containing liposomes, *J. Phys. Chem. B* **2015**, *119*, 1334-1349. https://doi.org/10.1021/jp5104752.
- (12) Kawai, C.; Prado, F. M.; Nunes, G. L. C.; Di Mascio, P.; Carmona-Ribeiro, A. M.; Nantes, I. L., pH-dependent interaction of cytochrome *c* with mitochondrial mimetic membranes: the role of an array of positively charges amino acids, *J. Biol. Chem.* **2005**, *280*, 34709-34717. https://doi.org/10.1074/jbc.M412532200.
- (13) Elmer-Dixon, M. M.; Bowler, B. E., Site A-mediated partial unfolding of cytochrome *c* on cardiolipin vesicles is species-dependent and does not require Lys72, *Biochemistry* **2017**, *56*, 4830–4839. <a href="https://doi.org/10.1021/acs.biochem.7b00694">https://doi.org/10.1021/acs.biochem.7b00694</a>.
- (14) Elmer-Dixon, M. M.; Bowler, B. E., Electrostatic constituents of cardiolipin interaction with site A of cytochrome *c*, *Biochemistry* **2018**, 57, 5683–5695. <a href="https://doi.org/10.1021/acs.biochem.8b00704">https://doi.org/10.1021/acs.biochem.8b00704</a>.
- (15) Steele, H. B. B.; Elmer-Dixon, M. M.; Rogan, J. T.; Ross, J. B. A.; Bowler, B. E., The human cytochrome *c* domain-swapped dimer facilitates tight regulation of intrinsic apoptosis, *Biochemistry* **2020**, *59*, 2055-2068. <a href="https://doi.org/10.1021/acs.biochem.0c00326">https://doi.org/10.1021/acs.biochem.0c00326</a>.
- (16) Rytömaa, M.; Kinnunen, P. K. J., Evidence for two distinct acidic phospholipid-binding sites in cytochrome *c*, *J. Biol. Chem.* **1994**, 269, 1770-1774. https://www.jbc.org/content/269/3/1770.
- (17) Sinibaldi, F.; Milazzo, L.; Howes, B. D.; Piro, M. C.; Fiorucci, L.; Polticelli, F.; Ascenzi, P.; Coletta, M.; Smulevich, G.; Santucci, R., The key role played by charge in the interaction of cytochrome c with cardiolipin, *JBIC*, *J. Biol. Inorg. Chem.* **2017**, *22*, 19–29.
- (18) Sinibaldi, F.; Howes, B. D.; Droghetti, E.; Polticelli, F.; Piro, M. C.; Di Pierro, D.; Fiorucci, L.; Coletta, M.; Smulevich, G.; Santucci, R., Role of lysines in cytochrome *c*–cardiolipin interaction, *Biochemistry* **2013**, *52*, 4578–4588. https://doi.org/10.1021/bi400324c.
- (19) Kostrzewa, A.; Páli, T.; Froncisz, W.; Marsh, D., Membrane location of spin-labeled cytochrome *c* determined by paramagnetic relaxation reagents, *Biochemistry* **2000**, *39*, 6066-6074.
- (20) Mohammadyani, D.; Yanamala, N.; Samhan-Arias, A. K.; Kapralov, A. A.; Stepanov, G.; Nuar, N.; Planas-Iglesias, J.; Sanghera, N.; Kagan, V. E.; Klein-Seetharaman, J., Structural characterization of

- cardiolipin-driven activation of cytochrome *c* into a peroxidase and membrane perturbation, *Biochim. Biophys. Acta Biomembr.* **2018**, *1860*, 1057-1068. https://doi.org/10.1016/j.bbamem.2018.01.009.
- (21) Pan, J.; Cheng, X.; Sharp, M.; Ho, C.-S.; Khadka, N.; Katsaras, J., Structural and mechanical properties of cardiolipin lipid bilayers determined using neutron spin echo, small angle neutron and X-ray scattering, and molecular dynamics simulations, *Soft Matter* **2015**, *11*, 130-138. https://doi.org/10.1039/C4SM02227K.
- (22) Bernad, S.; Oellerich, S.; Soulimane, T.; Noinville, S.; Baron, M. H.; Paternostre, M.; Lecomte, S., Interaction of horse heart and *Thermus thermophilus* type *c* cytochromes with phospholipid vesicles and hydrophobic surfaces, *Biophys. J.* **2004**, *86*, 3863-3872. https://doi.org/10.1529/biophysj.103.025114.
- (23) Hong, Y.; Muenzner, J.; Grimm, S. K.; Pletneva, E. V., Origin of the conformational heterogeneity of cardiolipin-bound cytochrome *c*, *J. Am. Chem. Soc.* **2012**, *134*, 18713-18723. <a href="https://doi.org/10.1021/ja307426k">https://doi.org/10.1021/ja307426k</a>.
- (24) Hanske, J.; Toffey, J. R.; Morenz, A. M.; Bonilla, A. J.; Schiavoni, K. H.; Pletneva, E. V., Conformational properties of cardiolipin-bound cytochrome *c, Proc. Natl. Acad. Sci. U.S.A.* **2012**, *109*, 125-130. https://doi.org/10.1073/pnas.1112312108.
- (25) Pandiscia, L. A.; Schweitzer-Stenner, R., Coexistence of native-like and non-native cytochrome *c* on anionic liposomes with different cardiolipin content, *J. Phys. Chem. B* **2015**, *119*, 12846-12859. https://doi.org/10.1021/acs.jpcb.5b07328.
- (26) Kusche, B. R.; Smith, A. E.; McGuirl, M. A.; Priestley, N. D., Alternating pattern of stereochemistry in the nonactin macrocycle is required for antibacterial activity and efficient ion binding, *J. Am. Chem. Soc.* **2009**, *131*, 17155-17165. https://doi.org/10.1021/ja9050235.
- (27) Pandiscia, L. A.; Schweitzer-Stenner, R., Salt as a catalyst in the mitochondria: returning cytochrome *c* to its native state after it misfolds on the surface of cardiolipin containing membranes, *Chem. Commun.* **2014**, 50, 3674-3676. https://doi.org/10.1039/c3cc48709a.
- (28) Blauer, G.; Sreerama, N.; Woody, R. W., Optical activity of hemoproteins in the Soret region. Circular dichroism of the heme undecapeptide of cytochrome *c* in aqueous solution, *Biochemistry* **1993**, *32*, 6674-9. https://doi.org/10.1021/bi00077a021.
- (29) Woody, R. W.; Hsu, M.-C., The origin of heme cotton effects in myoglobin and hemoglobin, *J. Am. Chem. Soc.* **1971**, *93*, 3515-3525. https://doi.org/10.1021/ja00743a036.
- (30) Pielak, G. J.; Oikawa, K.; Mauk, A. G.; Smith, M.; Kay, C. M., Elimination of the native Soret Cotton effect of cytochrome *c* by replacement of the invariant phenylalanine using site-directed mutagenesis, *J. Am. Chem. Soc.* **1986**, *108*, 2724-2727. <a href="https://doi.org/10.1021/ja00270a035">https://doi.org/10.1021/ja00270a035</a>.
- (31) Tsong, T. Y., The Trp-59 fluorescence of ferricytochrome c as a sensitive measure of the over-all protein conformation, *J. Biol. Chem.* **1974**, 249, 1988-1990.
- (32) Heimburg, T.; Marsh, D., Protein surface-distribution and protein-protein interactions in the binding of peripheral proteins to charged lipid membranes, *Biophys. J.* **1995**, *68*, 536-546. https://dx.doi.org/10.1016%2FS0006-3495(95)80215-8.

- (33) Pollock, W. B.; Rosell, F. I.; Twitchett, M. B.; Dumont, M. E.; Mauk, A. G., Bacterial expression of a mitochondrial cytochrome *c*. Trimethylation of Lys72 in yeast iso-1-cytochrome *c* and the alkaline conformational transition, *Biochemistry* **1998**, *37*, 6124-6131. https://doi.org/10.1021/bi972188d.
- (34) Diederix, R. E. M.; Ubbink, M.; Canters, G. W., The peroxidase activity of cytochrome *c*-550 from *Paracoccus versutus*, *Eur. J. Biochem.* **2001**, *268*, 4207-4216. https://doi.org/10.1046/j.1432-1327.2001.02335.x.
- (35) Elmer-Dixon, M. M.; Hoody, J.; Steele, H. B. B.; Becht, D. C.; Bowler, B. E., Cardiolipin preferentially partitions to the inner leaflet of mixed lipid large unilamellar vesicles, *J. Phys. Chem. B* **2019**, *123*, 9111–9122. <a href="https://doi.org/10.1021/acs.jpcb.9b07690">https://doi.org/10.1021/acs.jpcb.9b07690</a>.
- (36) Paradisi, A.; Bellei, M.; Paltrinieri, L.; Bortolotti, C. A.; Di Rocco, G.; Ranieri, A.; Borsari, M.; Sola, M.; Battistuzzi, G., Binding of *S. cerevisiae* iso-1 cytochrome *c* and its surface lysine-to-alanine variants to cardiolipin: charge effects and the role of the lipid to protein ratio, *JBIC*, *J. Biol. Inorg. Chem.* **2020**, *25*, 467-487. <a href="https://doi.org/10.1007/s00775-020-01776-1">https://doi.org/10.1007/s00775-020-01776-1</a>.
- (37) Mandal, A.; Hoop, C. L.; DeLucia, M.; Kodali, R.; Kagan, V. E.; Ahn, J.; van der Wel, P. C. A., Structural changes and proapoptotic peroxidase activity of cardiolipin-bound mitochondrial cytochrome *c*, *Biophys. J.* **2015**, *109*, 1873-1884.
- (38) Gilkerson, R. W.; Selker, J. M. L.; Capaldi, R. A., The cristal membrane of mitochondria is the principal site of oxidative phosphorylation, *FEBS Lett.* **2003**, *546*, 355-358.
- (39) Mannella, C. A., The relevance of mitochondrial membrane topology to mitochondrial function, *Biochim. Biophys. Acta* **2006**, *1762*, 149-147.
- (40) Porcelli, A. M.; Ghelli, A.; Zanna, C.; Pinton, P.; Rizzuto, R.; Rugolo, M., pH difference across the outer mitochondrial membrane measured with a green fluorescent protein mutant, *Biochem. Biophys. Res. Commun.* 2005, 326, 799-804. https://doi.org/10.1016/j.bbrc.2004.11.105.
- (41) Duncan, M. G.; Williams, M. D.; Bowler, B. E., Compressing the free energy range of substructure stabilities in iso-1-cytochrome *c*, *Protein Sci.* **2009**, *18*, 1155-1164. https://doi.org/10.1002/pro.120.
- (42) Margoliash, E.; Frohwirt, N., Spectrum of horse-heart cytochrome *c*, *Biochem*. *J*. **1959**, *71*, 570-572. https://doi.org/10.1042/bj0710570.
- (43) Elmer-Dixon, M. M.; Bowler, B. E., Rapid quantification of vesicle concentration for DOPG/DOPC and Cardiolipin/DOPC mixed lipid systems of variable composition, *Anal. Biochem.* **2018**, *553*, 12-14.
- (44) Elmer-Dixon, M. M.; Bowler, B. E., Rapid quantification of cardiolipin and DOPC lipid and vesicle concentration, *Anal. Biochem.* **2017**, *520*, 58-61.

Table of Contents (TOC) graphic (for Table of Contents only):

